Dependence of Induced Transmembrane Potential on Cell Density, Arrangement, and Cell Position Inside a Cell System

Mojca Pavlin, Nataša Pavšelj, and Damijan Miklavčič*

Abstract—A nonuniform transmembrane potential (TMP) is induced on a cell membrane exposed to external electric field. If the induced TMP is above the threshold value, cell membrane becomes permeabilized in a reversible process called electropermeabilization. Studying electric potential distribution on the cell membrane gives us an insight into the effects of the electric field on cells and tissues. Since cells are always surrounded by other cells, we studied how their interactions influence the induced TMP. In the first part of our study, we studied dependence of potential distribution on cell arrangement and density in infinite cell suspensions where cells were organized into simple-cubic, body-centered cubic, and face-centered cubic lattice. In the second part of the study, we examined how induced TMP on a cell membrane is dependent on its position inside a three-dimensional cell cluster. Finally, the results for cells inside the cluster were compared to those in infinite lattice. We used numerical analysis for the study, specifically the finite-element method (FEM). The results for infinite cell suspensions show that the induced TMP depends on both: cell volume fraction and cell arrangement. We established from the results for finite volume cell clusters and layers, that there is no radial dependence of induced TMP for cells inside the cluster.

Index Terms—Cell cluster, cell suspension, electropermeabilization, finite-element modeling, transmembrane potential.

I. INTRODUCTION

EXTERNAL electric field causes biochemical and physiological changes in biological cells and tissues. When an electric field is applied to a cell or cell system, a nonuniform transmembrane potential (TMP) is induced on exposed cells. If the induced TMP is large enough, i.e., above the threshold value (TMP_c), the cell membrane becomes permeabilized in a reversible process called electropermeabilization, thus allowing entrance of molecules that otherwise cannot easily cross the cell membrane [1]–[3]. Further increase of the electric field causes irreversible membrane permeabilization and cell death. Induced TMP in biological cells exposed to electromagnetic fields is of interest in a variety of applications, such as gene transfection [4], electrochemotherapy [5], the study of forces on cells undergoing fusion, models of cardiac tissue response to defibrilating currents, and the study of potential health effects of electric and magnetic fields [6], [7]. Therefore, investigation of induced potential distribution on the cell membrane is important in studying the effects of the electric field on biological cells.

Potential distribution on the surface of a cell placed in an electric field can be calculated analytically or numerically. Even though analytical solutions are possible only for some analytically defined shapes, such us spheroids [8], they give us a rough picture of the dependence of the induced TMP on electric and geometric parameters.

In the spherical coordinate system, a cell can be represented by a sphere surrounded with a shell. In Fig. 1, we see a cross section of such a sphere.

A cell membrane is shown as a shell, where d denotes membrane thickness and R the cell radius. Membrane thickness is exaggerated for easier representation. σ_e and σ_i represent specific conductivity of the external and the internal medium, respectively, and σ_m represents specific conductivity of the membrane. θ is an angle measured with respect to the electric field direction. Analytical solution for static case for induced TMP is given by Schwan's equation [9]

$$\Delta\Psi = \text{TMP} = g(\lambda)E_0 R \cos\theta \qquad (1)$$

where $\Delta\Psi$ represents potential drop across the cell membrane. Factor $g(\lambda)$ is a function of cell parameters and E_0 is the applied electric field. For physiological conditions where $d \ll R$ and $\sigma_m \ll \sigma_e, \sigma_i$, [10], (1) simplifies to
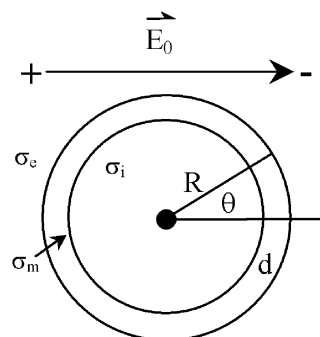
$$\text{TMP} = 1.5 R E_0 \cos\theta \qquad (2)$$

Fig. 1. Model of a cell, where σ_e, σ_i and σ_m represent specific conductivities of external medium, internal medium and cell membrane, respectively, θ is an angle measured with respect to the electric field direction (E_0), R denotes cell radius and d membrane thickness.

which is an exact solution for potential on a surface of a nonconducting sphere. However, for low conducting media the exact equation (1) has to be applied [11].

In majority of experiments, cells are surrounded by other cells, so the aim of this study was to get an insight into cell interactions in monolayers, suspensions, aggregates, clusters and tissues and how this influences the induced TMP. Each cell in electric field behaves as a dipole, which modifies external electric field. Mutual interactions between dipoles lead to problem of many-body system for which analytical solutions are too complex to obtain [12]–[14]. Therefore, numerical methods have to be applied to obtain the solution for field distribution and induced TMP in cell suspensions and cell clusters. In this paper, we shall limit ourselves only to the analysis for the static direct current, which holds also for the frequencies under the relaxation frequency (approximately 1 MHz). To obtain the solution for higher frequencies one has to consider also the dielectric properties of the cell, however in the low frequency range the conductive properties of the cells are dominant.

In the first part of our study, we modeled infinite cell suspensions where cells were arranged into simple-cubic (sc), body-centered cubic (bcc), and face-centered cubic (fcc) lattice. We studied the influence of cell arrangement and density on induced TMP distribution in a cell membrane. We also calculated fraction of a cell surface where the induced TMP is above the threshold value (TMP_c) for different cell densities and arrangements.

In the second part of our study, we studied three-dimensional cell clusters as models of multicellular tumor spheroids [15]. A multicellular tumor spheroid is an *in vitro* model of a real tumor, used for studying molecular transport, cell viability and electroporation protocols in tumors. We examined how induced TMP in a cell depends on its position inside a cluster. Finally, we compared the results for cells inside the cluster to those in infinite lattice, i.e., cell suspensions.

II. METHODS

A. Finite-Element Modeling

Since the analytical equations are too complex for problem of many interacting cells, we used numerical analysis for the study. Numerical calculations were performed by finite-element modeling software EMAS (Ansoft, Pittsburgh, PA), using finite-element method (FEM). Details of this program and FEM method are described elsewhere [16]. Briefly, FEM solves partial differential equation by dividing the volume into smaller elements and solving differential equation on elements. These elements have various shapes and sizes so that complex geometries can be modeled. Resolution of the model is increased by increasing number of elements. The maximum number of elements, however, is limited by the computer memory capacity.

B. Models

Biological cells were modeled as nonconductive spheres, since under normal conditions membrane conductivity is many orders smaller than that of the external medium and, therefore, can be neglected [10]. Cells were organized either into sc, bcc, or fcc lattice shown in Fig. 2. Using the symmetry of cubic
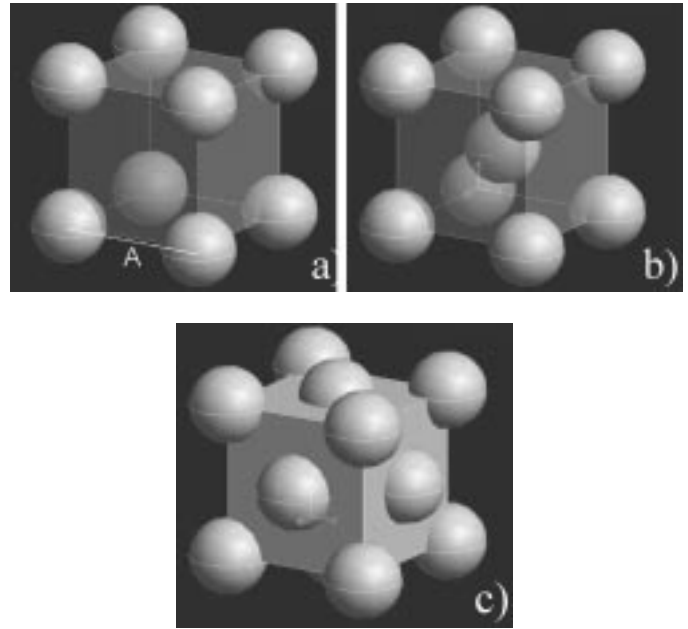

Fig. 2. Unit cells for (a) sc, (b) bcc, and (c) fcc lattices. A is length of unit cell side shown in (a).

lattices and applying appropriate boundary conditions, we were able to model infinite cubic lattices with a model of a primitive cell.

We studied the difference in the induced TMP distribution between infinite lattice arrangements for two cases. To compare our results with our previous work [17], we first calculated the induced TMP for different packing ratios (PRs). The PR was defined as a ratio of cell distance to cell diameter. Second, we analyzed differences in induced TMP for different volume fractions. Volume fraction is defined as a percentage of volume occupied by cells [see (9) in the Appendix]. The relation between volume fraction and PR for the simple cubic lattice is given by

$$f_{\mathrm{sc}} = \frac{4\pi}{3} \cdot \left(\frac{R}{2(1+\mathrm{PR}_{\mathrm{sc}})} \right)^3 \qquad (3)$$

and can be easily calculated from geometry of the unit cells (Fig. 2). To get a better idea of the relation between the two parameters, we calculated PRs for given volume fraction for the sc lattice. The conversion is in Table I.

For the bcc and fcc arrangement, however, the PR cannot be uniquely defined, therefore, PR is not adequate parameter for this study. On the other hand, volume fraction is usually the parameter that gives us information about the cell density and is also the only factor contributing to equivalent conductivity of an array of cells [12], [18], [19]. Therefore, we compared the induced TMP for different lattices for the same volume fraction—f. Varying sphere radius calculations were performed for different cell volume fraction f, where $f = 4\pi/3N(R/A)^3$, where A is the length of the unit cell side shown in Fig. 2(a) and N number of the spheres in the unit cell. Maximum volume fractions for hard spheres are 0.52 for sc, 0.64 for bcc, and 0.74 for fcc lattice.

It was suggested in the literature [20] that permeabilization is linearly proportional to the area above the TMP_c. We, therefore,

TABLE I
CONVERSION BETWEEN VOLUME FRACTION AND PR FOR SC LATTICE

volume fraction f*	PR sc
0.01	2.741
0.05	1.188
0.1	0.736
0.3	0.204
0.5	0.015

*from (3)

calculated fraction of the cell surface having the induced TMP above the threshold value TMP_c, which was chosen within the range reported in the literature (200–1000 mV) [2], [21]–[25].

Dependency of induced TMP on angle θ was fitted with a polynomial of third order $p(\theta)$ with least square method. Critical angle θ_c can be defined as the angle where threshold value for permeabilization is reached

$$\mathrm{TMP}_c/E_0R = p(\theta_c). \tag{4}$$

From the critical angle the permeabilized area was calculated with

$$S_c/S_0 = (1 - \cos\theta_c) \qquad \text{(where } S_0 = 4\pi R^2\text{).} \tag{5}$$

In the second part of the study, we analyzed cell clusters as models of multicellular tumor spheroids [15]. Potential and electric field distribution around a densely packed cell cluster is similar to the distribution around a single isolated cell. When defining the boundary conditions of the model, we must ensure that the boundary placement does not influence the electric field in the cluster. Again, cubic symmetry enabled us to model the whole cluster by calculating only its one-fourth. In Fig. 3, we see the whole cluster, where 675 cells (seven cells or approximately 140 μm in diameter) were arranged in fcc lattice as close to spherical shape as possible. In multicellular tumor spheroids, cells are tightly packed ($f = 0.46$–0.65) [26]–[28] so we chose fcc lattice, because it is the arrangement where the highest volume fraction of cells is possible (up to 0.74).

Unless otherwise specified, all results for the induced TMP are normalized to the applied electric field magnitude and cell radius.

III. RESULTS AND DISCUSSION

A. Cell Suspensions

In this first part of the study, we analyzed how induced TMP depends on cell arrangement and volume fraction. We first calculated the induced TMP for the simple cubic lattice for different PRs. For the PR $= 0$, we obtained the decrease of factor 1.5 to 1.0 which was already shown previously [17]. However, for further analysis we analyzed the induced TMP for different volume fractions [for correlation between PR and volume fraction see (3) and Table I]. In Fig. 4, we show the results for sc, bcc,
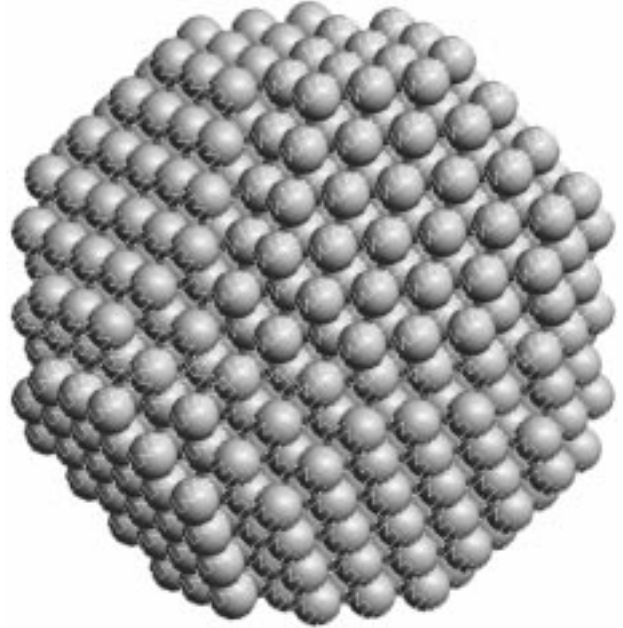

Fig. 3. Model of a cell cluster representing multicellular tumor spheroid, composed of 675 cells arranged in fcc lattice.

and fcc lattices having the same volume fraction. Since maximum volume fraction for hard spheres arranged in sc lattice is 0.52, we were able to compare three different arrangements studied up to $f = 0.52$.

As reported previously [17], a change in induced TMP distribution on cell membrane and a decrease of its maximum value was observed in cell suspensions. These changes are due to interaction with neighboring cells.

We can see from Fig. 4 that induced TMP depends not only on the volume fraction, but also on cell arrangement inside the lattice (sc, bcc, or fcc) which can be explained with different number of nearest neighbors and different cell arrangement in different lattices. Therefore, the induced TMP depends on both; on cell volume fraction and cell arrangement.

In real suspensions, cells arrange randomly or under the gravitational force. For volume fractions above 0.52, cells can order only in bcc and fcc lattices, and above 0.62 only the latter is possible. Hexagonal packing is also possible but since this arrangement is similar to fcc we presumed that fcc lattice is the most representative.

We then calculated fraction of the cell surface having the induced TMP above the threshold value TMP_c for the hexagonal packing. The fraction of permeabilized area was obtained with (5) derived in the Methods section. The results for the fraction of permeabilized area are represented in Fig. 5.

The fraction of permeabilized area decreases with increasing volume and depends on the critical TMP. Therefore, efficiency of electroporation depends also on cell density.

In all our calculations, we neglected the resting potential of the cell. In literature, there is a general agreement that induced TMP is superimposed on the resting potential [21]. The critical voltage for membrane permeabilization was reported to be in the range from 200 up to 1000 mV while the resting potential is between 50 and 100 mV for excitable cells and even lower for
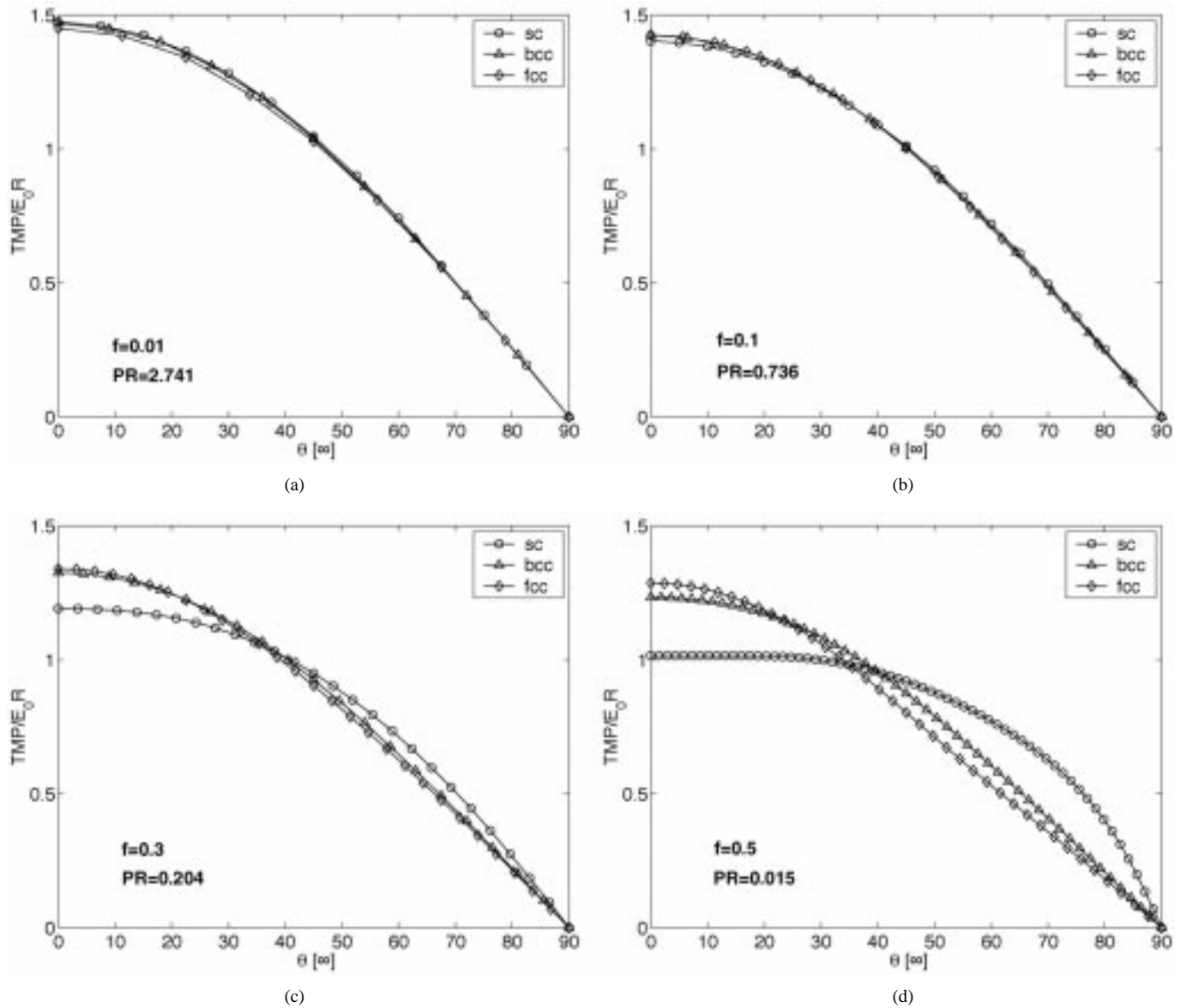
Fig. 4. Comparison of induced TMP, normalized to electric field magnitude and cell radius, on cells in suspensions arranged in sc, bcc, fcc lattice for volume fractions $f = 0.01$, 0.1, 0.3, and 0.5.

non excitable cells as chinese hamster lung cells (20–29 mV) [22]. Therefore, TMP is increased on one side of the cell and decreased on the other in the range of 5% to 50%. If the induced TMP is under critical value on larger part of the cell the change due to resting potential has no significant effect on the fraction of permeabilized area since the smaller fraction on one side of the cell is compensated with larger area on the other side. However, if the maximum induced TMP is just above the critical value, the effect of increased TMP on one side of the cell is significant and should be taken into account.

B. Cell Clusters

In the second part of our study, we observed induced TMP on cells in the mid section plane of the cluster, parallel to the field direction. As mentioned before, we only modeled one-fourth of the cluster, due to the symmetry of the model. We chose electric field magnitude outside the cluster to be 1 MV/m, which is

quite large in terms of cell permeabilization, but since the model is linear, the results can easily be scaled to the electric field magnitude of interest. We analyzed induced TMP values on the cells in a cross section of the cluster. The average maximum induced TMP inside the cluster for cell diameter 16 μm was 11.24 V (induced TMP scaled to 500 mV corresponds to 44.5 kV/m of applied field). We noticed some small differences between the cells inside the cluster. But these differences are in the range of 1% and are most probably due to numerical calculations. However, we noticed larger deviations in the induced TMP for the cells on the edge of the cluster. We established that there is no radial dependence of induced TMP except for those small differences in the outer cells. This can be attributed to the fact that the cluster deviates from spherical shape. In order to confirm this, we amplified this effect by building an FEM model of a layer of cells, with large irregularities in circular shape. We removed some cells from the circular layer. Deviations of induced TMP
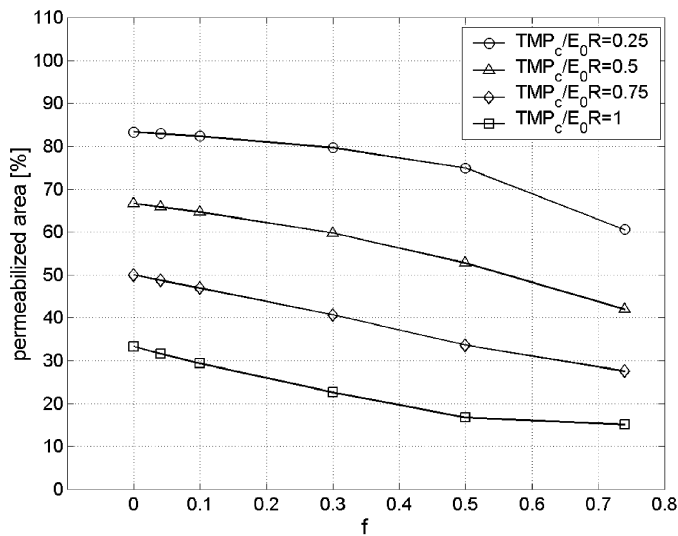
Fig. 5. Percentage of permeabilized area for fcc lattice for different normalized critical TMPs. For TMP_c given in range reported in literature (0.25–1 V) and for a typical cell size ($R \sim 10\,\mu$m) is $E_0 \sim 100$ kV/m. For $f = 0$, we have the case of an isolated cell.

are shown in Fig. 6, where for easier presentation only the deviations above 2% are shown. We can see that deviations in induced TMP are much amplified for the cells near the irregularities.

To better understand why the position of a cell inside the cluster does not play any role in the cell's induced TMP, we built a model where a cluster of cells was represented with a sphere having an equivalent conductivity. To calculate equivalent conductivity of the cluster—σ we used Maxwell equation [19], [29], [30] (see the Appendix) and by inserting $\sigma_p = 0$ for conductivity of a cell into (8), we obtain

$$\sigma/\sigma_e = \frac{1 - f}{1 + 0.5f} \quad (6)$$

where parameter f is volume fraction of cells in cluster and σ_e is extracellular conductivity.

Electric field inside the cluster depends only on the ratio between equivalent and external conductivity [10], [9]

$$E = \frac{3\sigma_e}{2\sigma_e + \sigma}. \quad (7)$$

According to (6) and (7), average electric field inside the cluster increases, due to the decrease of equivalent conductivity.

In Fig. 7(a), we see equipotential planes of this model. Equipotentials inside the sphere are equidistant, the electric field is homogeneous and, therefore, all the cells inside the sphere have the same induced TMP. However, in reality a cluster of cells is never a perfect sphere, so we can observe irregularities for the cells on the edge. To illustrate this, we built a model that has four irregularities: two hollows and two knobs, one on the side that is parallel and the other on the side of the cluster that is perpendicular to the electric field. In Fig. 7(b), we can see how the homogeneity of the electric field is deformed near the irregularities. In a cluster of cells, such irregularities lead to the deviation of induced TMP for the cells in these areas from centrally located cells.
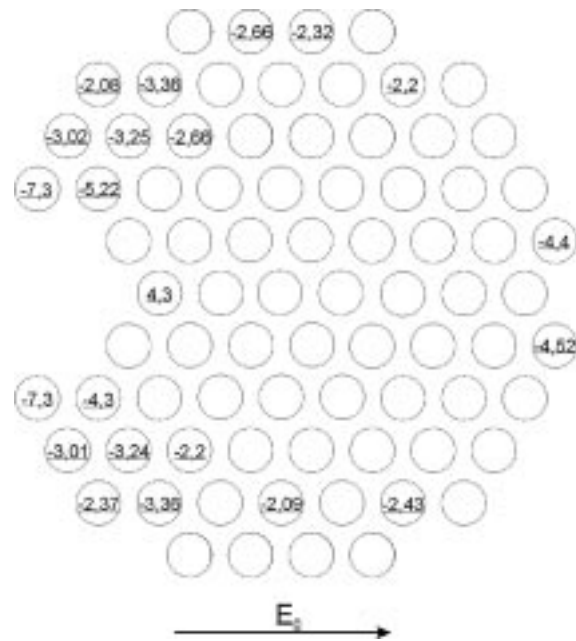

Fig. 6. A model of a layer of cells with large irregularities. Layer is arranged into hexagonal lattice (not fcc), which enables us to even better approximate circular shape. The deviations from the average middle cell are shown in percentage.
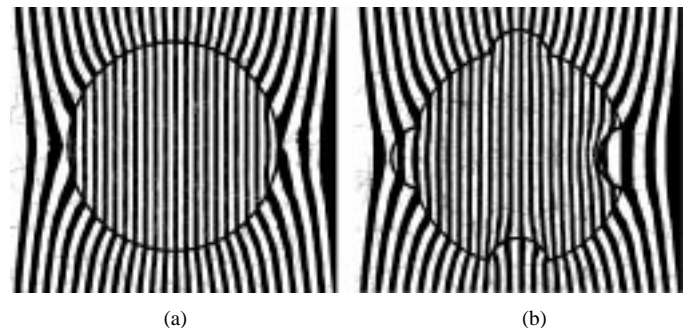

Fig. 7. Equipotentials of models, where a cluster of cells is represented with equivalent conductivity (a) a cluster is represented with a perfect sphere, (b) a cluster with irregularities in spherical shape.

Volume fraction of our cell cluster was 0.38, which is a little lower than the volume fraction of real multicellular spheroids (0.45–0.65), but unfortunately we were limited with computer memory capacity. We analyzed induced TMP inside the cluster and its radial dependency. If we compare values of normalized induced TMP in the strand of cells in the middle of the cluster, parallel to the electric field direction, we can see there is no radial dependency, except for small differences for the outer two cells. We can also notice a drop of factor 1.5 in (1) (for an isolated cell) to approximately 1.4, which can be explained by two contributing effects acting in opposite directions. First, an increase of average electric field inside the cluster due to lower equivalent conductivity of the cluster [(6) and (7)]. And second, a decrease of induced TMP is observed and described for infinite lattices of cells (Fig. 4) because of a decrease of local electric field inside the cluster, due to interactions between cells.

We compared the results of the cluster with those for infinite lattice having the same density and cell arrangement. The comparison is shown in Fig. 8(a). It should be stressed that in

order to normalize the calculated TMP inside the cluster, we used the average field E inside the cluster, which is higher than the applied field E_0 ($E_{\text{numerical}} = 1.13\, E_0$). The calculation of the average field E inside the cluster is shown in Fig. 8(b). We can see that equipotential surfaces follow the symmetry of the fcc lattice. By determining the potential difference between two symmetric points, the average field inside the cluster was calculated. We also calculated field E inside the cluster theoretically, according to (7) for equivalent sphere. However, we obtained a slightly different result ($E_{\text{theoretical}} = 1.2\, E_0$) due to the fact that one cannot assign a discrete border to a cluster. Therefore, equipotentials bend slightly on the border of a real cluster and are not straight as they are in equivalent sphere [see Fig. 7(a)].

In Fig. 8(a), we compared the results for cells arranged in infinite fcc lattice with the results for cells in cluster normalized to local electric field—E for both cases—the field obtained numerically and theoretically [Fig. 8(b)]. We can see that there is no observable difference between the numerically obtained results for the cluster and the infinite lattice. In this way, we also demonstrated that induced TMP of a cell inside the cluster depends on local field and not on its position inside the cluster. The only change is observed on the border of the cluster where local electric field is changed. Therefore, we can conclude that cluster size does not have any impact on induced TMP for cells inside the cluster, provided that cell density and size throughout the cluster are uniform.

IV. CONCLUSION

In our study, we used finite-elements modeling to study induced TMP dependence on cell arrangement, volume fraction and PR. As models of cell suspensions in the first part of the study, we used infinite array of cells arranged into sc, bcc, and fcc lattices. In the second part of the study, we used cell clusters as models of multicellular tumor spheroids. From the theory of dispersed systems we know that bulk conductivity depends on volume fraction—density of cells in suspension [19]. So one might expect that volume fraction has a direct proportional effect on induced TMP as well. However, we showed that volume fraction and cell arrangement both influence the induced TMP. It should be stressed that our calculations are valid for cells that are not electrically connected which is true for cell suspensions and multicellular tumor spheroids as *in vitro* models of tumors [15]. For the tissue cells and cells that are electrically connected with gap junctions (epithelial tissues, nerve, and cardiac cells), other approaches have to be used [6], [7].

In all our calculations, we neglected resting TMP. We limited our calculations to a dc case, which holds also for the frequencies under the relaxation frequency—about 1 MHz.

In real suspensions, cells order randomly so that cells are as far as possible from each other, therefore, fcc lattice is probably the closest approximation to real suspensions. We showed that for fcc lattice we get considerable decrease in induced TMP compared to Schwan equation for isolated cell (up to 15%) and fraction of permeabilized area (up to 50%). For other arrangements of cells, even larger decrease is obtained.

As we see from the results for cell clusters and layers, there is no radial dependence inside the finite arrangements of cells.
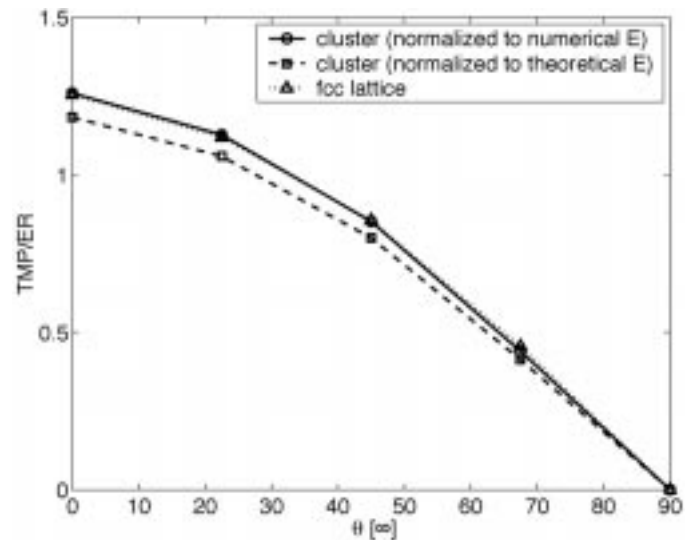
(a)
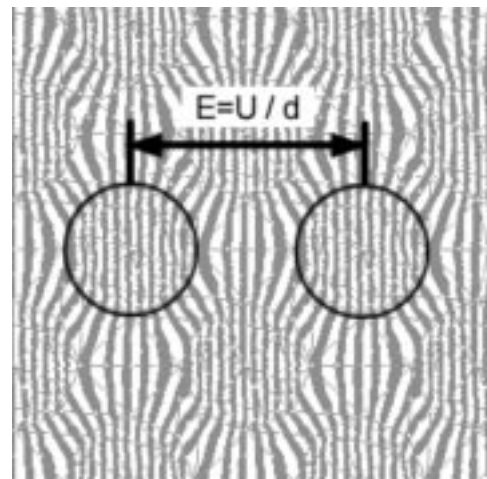
(b)

Fig. 8.　(a) Comparison of finite-volume fcc cell cluster and infinite fcc lattice, E is the average field inside the cell cluster for both cases-obtained numerically and theoretically, R is the cell radius. For infinite lattice, $E = E_0$. (b) Calculation of the average field E inside the cluster.

But it has to be emphasized that this is only true for the homogeneous arrangements of cells that can be represented with a sphere having equivalent homogeneous conductivity. We observed small differences in induced TMP on the border of a cluster are due to the fact that clusters deviate from spherical shape, which alters electric field on the border of a cluster.

Finally, we analyzed values of induced TMP inside the cluster. We showed that the drop of factor g from 1.5 for isolated cell [(1) and (2)] to approximately 1.4 for the case of fcc lattice with volume fraction 0.38, can be explained by two contributing factors having the opposite effects. First, an increase of the electric field inside the cluster due to the decrease in equivalent conductivity, and second, a decrease of induced TMP due to interaction between the cells. We verified this by comparing induced TMP between the cells that are arranged in infinite lattice and those inside a finite cluster of cells. Taking into account both contributing factors for cells in clusters we obtained the same result as for cells arranged in infinite lattice.
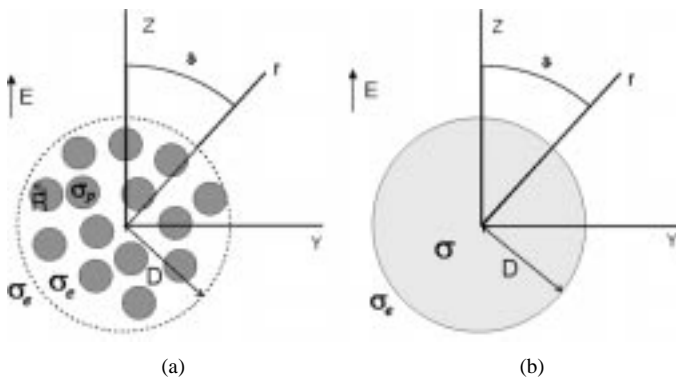
Fig. 9. Maxwell's derivation of conductivity for dilute suspension of particles. (a) N spheres dispersed in medium that induces the same potential under external field E as (b) one sphere of radius D having effective conductivity σ.

Drawback of our approach is that using FEM method we were not able to model a suspension or a multicellular spheroid of randomly dispersed cells such as in realistic suspensions and spheroids. Also, the size of cells can vary, so the reality is somewhat different from the ideal case of our study. Size and density of our cell clusters though was in the range of the size and the density of real multicellular tumor spheroids. The models we used in our study are in fact very idealized, but as such give us an answer to our question: Does a cell position inside the cluster itself, not taking into account the distribution of cells and their size, have any effect on induced TMP in a cell?

From literature we know [12]–[14] that random or ordered arrangement does not significantly change effective conductivity, but for calculations of TMP this could be of some importance. Also, for more accurate result of fraction of permeabilized area, membrane resting potential should be taken into account.

In summary, we showed that for evaluation of experimental results one should consider deviation of induced TMP due to cell arrangement, especially for dense cell suspensions and multicellular spheroids. For experiments on multicellular tumor spheroids, it is also necessary to evaluate changes around nonhomogenates (deviations from round shape) which alter induced TMP on the border of a tumor.

APPENDIX

A. Maxwell Equation

Maxwell was first to derive the equation for effective conductivity σ of dilute suspension [29], [30]. He realized that potential due to N spheres lying in external field having conductivity σ_p and dispersed in medium σ_e [Fig. 9(a)] is equal to the potential of equivalent sphere having effective conductivity σ [Fig. 9(b)]. With this he derived his equation

$$\frac{\sigma_e - \sigma}{2\sigma_e + \sigma} = f \frac{\sigma_e - \sigma_p}{2\sigma_e + \sigma_p}. \tag{8}$$

Parameter f is volume fraction of particles dispersed in medium and is defined as

$$f = \frac{NR^3}{D^3} \tag{9}$$

where D denotes radius of equivalent sphere. The parameter f indicates how tightly the cells are packed together and can range from nearly zero (dilute suspensions) up to 0.74 (maximum for spherical cells).

It was shown experimentally [10] and numerically [19] that for suspensions of nonconductive particles Maxwell equation is valid also for volume fractions up to 0.74.

REFERENCES

[1] L. M. Mir, "Therapeutic perspectives of *in vivo* cell electropermeabilization," *Bioelectrochemistry*, vol. 53, pp. 1–10, 2000.

[2] E. Neumann, A. E. Sowers, and C. A. Jorda, *Electroporation and Electrofusion in Cell Biology*. New York: Plenum, 1989.

[3] S. Orlowski and L. M. Mir, "Cell electroporation: A new tool for biochemical and pharmacological studies," *Biochim. Biophys. Acta*, vol. 1154, pp. 51–62, 1993.

[4] L. M. Mir, M. F. Bureau, J. Gehl, R. Rangara, D. Rouy, J. M. Caillaud, P. Delaere, D. Branellec, B. Schwartz, and D. Scherman, "High-efficiency gene transfer into skeletal muscle mediated by electric pulses," in *Proc. Nat. Acad. Sci. USA*, vol. 96, 1999, pp. 4262–4267.

[5] G. Sersa, T. Cufer, M. Cemazar, M. Rebersek, and Z. Rudolf, "Electrochemotherapy with bleomycin in the treatment of hypernephroma metastasis," *Case Report and Literature Review, Tumori*, vol. 86, pp. 163–165, 2000.

[6] C. E. Fear and M. A. Stuchly, "Biological cells with gap junctions in low-frequency electric fields," *IEEE Trans. Biomed. Eng.*, vol. 45, pp. 856–866, July 1998.

[7] ——, "Modeling assemblies of biological cells exposed to electric fields," *IEEE Trans. Biomed. Eng.*, vol. 45, pp. 1259–1271, Oct. 1998.

[8] T. Kotnik and D. Miklavčič, "Analytical description of transmembrane voltage induced by electric fields on spheroidal cells," *Biophys. J.*, vol. 79, pp. 670–679, 2000.

[9] H. P. Schwan, "Electrical properties of tissue and cell suspensions," *Adv. Biol. Med. Phys.*, vol. 5, pp. 147–209, 1957.

[10] C. Polk and E. Postow, "Dielectric properties of tissues," in *Handbook of Biological Effects of Electromagnetics Fields*, 2nd ed, C. Polk and E. Postow, Eds. Boca Raton, FL: CRC, 2000, pp. 28–92.

[11] T. Kotnik, F. Bobanović, and D. Miklavčič, "Sensitivity of transmembrane voltage induced by applied electric fields—A theoretical analysis," *Bioelectrochem. Bioen.*, vol. 43, 1997.

[12] S. S. Dukhin, "Dielectric properties of disperse systems," in *Surface and Colloid Science*, E. Matijević, Ed. New York: Wiley-Interscience, 1971, vol. 3, pp. 83–165.

[13] S. Takhasima, *Electrical Properties of Biopolimers and Membranes*. Bristol, U.K.: Adam Hilger, 1989.

[14] T. Hanai, "Electrical properties of emulsions," in *Emulsion Science*, P. Sherman, Ed. London, U.K.: Academic Press, 1968, pp. 353–478.

[15] R. M. Sutherland, "Cell and environment interactions in tumor microregions: The multicell spheriod model," *Science*, vol. 240, pp. 177–184, 1988.

[16] D. Šemrov and D. Miklavčič, "Numerical modeling for *in vivo* electroporation," in *Electrochemotherapy, Electrogenetherapy and Transdermal Drug Delivery: Electrically Mediated Delivery of Molecules to Cells*, M. J. Jaroszeski, R. Heller, and R. Gilbert, Eds. Totowa, NJ: Humana, 1999, pp. 63–81.

[17] R. Susil, D. Šemrov, and D. Miklavčič, "Electric field—Induced transmembrane potential depends on cell density and organization," *Electro. Magnetobiol.*, vol. 17, no. 3, pp. 391–399, 1998.

[18] L. Rayleigh, "On the influence of obstacle arranged in rectangular order upon the properties of a medium," *Phil. Mag.*, vol. 34, pp. 481–502, 1892.

[19] M. Pavlin, T. Slivnik, and D. Miklavčič, "Effective conductivity of cell suspensions," *IEEE Trans. Biomed. Eng.*, vol. 49, pp. 77–80, Jan. 2002.

[20] B. Gabriel and J. Teissie, "Fluorescence imaging in the millisecond time range of membrane electropermeabilization of single cells using a rapid ultra-low-light intensifying detection system," *Eur. Biophys. J.*, vol. 27, pp. 291–298, 1998.

[21] U. Zimermann, "Electric field-mediated fusion and related electrical phenomena," *Biochimica et Biophysica Acta*, vol. 694, pp. 227–277, 1982.

[22] H. G. Sachs, P. J. Stambrook, and J. D. Ebert, "Changes in membrane potential during the cell cycle," *Exp. Cell Res.*, vol. 83, pp. 2362–2666, 1974.

[23] D. Miklavčič, D. Šemrov, H. Mekid, and L. M. Mir, "A validated model of *in vivo* electric field distribution in tissues for electrochemotherapy and for DNA electrotransfer for gene therapy," *Biochim. Biophys. Acta*, vol. 1519, pp. 73–83, 2000.

[24] M. Hibino, M. Shigemori, H. Itoh, K. Nagayama, and K. Kinosita, Jr., "Membrane conductance of an electroporated cell analyzed by submicrosecond imaging of transmembrane potential," *Biophys. J.*, vol. 59, pp. 209–220, 1991.

[25] J. Tessie and M. Rols, "An experimental evaluation of the critical potential difference inducing cell membrane electropermeabilization," *Biophys. J.*, vol. 65, pp. 409–413, 1993.

[26] R. K. Jain, "Barriers to drug delivery in solid tumors," *Scientif. Amer.*, pp. 42–49, July 1994.

[27] A. C. Guyton and J. E. Hall, *Tekstbook of Medical Physiology—Ninth Edition. Unit IV—The Circulation & Unit V—The Kidneys and Body Fluids*. Philadelphia, PA: Saunders, 1996.

[28] I. F. Tannock and R. P. Hill, *The Basic Science of Oncology—Third Edition*. New York: McGraw-Hill, 1998.

[29] J. C. Maxwell, *Treatise on Electricity and Magnetism*. London, U.K.: Oxford Univ. Press, 1873.

[30] V. H. Pauly and H. P. Schwan, "Über die Impendanc einer Suspension von kugelförmigen teilchen mit einer Schale," *Z. Naturforschg*, vol. 14b, pp. 125–131, 1959.

Mojca Pavlin was born in 1973 in Ljubljana, Slovenia. She received the B.Sc. degree in physics from the University of Ljubljana, Faculty of Mathematics and Physics in 1998 and the M.Sc. degree from the Faculty of Electrical Engineering in 2001. She is working towards the Ph.D. degree in electrical engineering at the University of Ljubljana.

Her main research interests lie in the field of biophysics, especially in the analysis of the interactions of the electric fields and many cells systems including numerical modeling and experimental work on cells.

Nataša Pavšelj was born in 1974 in Ljubljana, Slovenia. She received the B.Sc. degree in electrical engineering from the University of Ljubljana, Faculty of Electrical Engineering in 1999 and is currently a researcher working towards the M.Sc. degree at the Faculty of Electrical Engineering.

Her main research interests lie in the field of electroporation, including numerical modeling of electric field distribution in different biological tissue setups and cell systems, and comparison of the theoretical results with the experimental work.

Damijan Miklavčič was born in 1963 in Ljubljana, Slovenia. He received the M.Sc. and Ph.D. degrees in electrical engineering from University of Ljubljana.

Since 1997, he is an Associate Professor at Faculty of Electrical Engineering, University of Ljubljana, and the Head of Laboratory of Biocybernetics. He works in the field of biomedical engineering. His interest in the last years focuses on electroporation assisted drug delivery, including cancer treatment by means of electrochemotherapy, tissue oxygenation, and modeling.